Science of the Total Environment 831 (2022) 154924

Contents lists available at ScienceDirect

Science of the Total Environment

journal homepage: www.elsevier.com/locate/scitotenv

Surface-subsurface hydrological processes of rainwater harvesting project in karst mountainous areas indicated by stable hydrogen and oxygen isotopes

Fan Liu [a,b,c], Guanghui Jiang [b,c,*], Guangcai Wang [a], Fang Guo [b,c], Jia Wang [b,c], Qigang Wang [b], Jie Shi [b], Jingyi Cai [d], Min Wang [a]

[a] School of Water Resources and Environment, China University of Geosciences, Beijing 100083, China
[b] Key Laboratory of Karst Dynamics, MNR/GZAR, Institute of Karst Geology, Chinese Academy of Geological Sciences, Guilin 541004, China
[c] Guangxi Karst Resources and Environment Research Center of Engineering Technology, Guilin 541004, China
[d] Hebei Investigation Institute of Hydrogeology and Engineering Geology, Shijiazhuang 050021, China

HIGHLIGHTS

- Study the rainwater harvesting projects in karst mountains from runoff components.
- Evapotranspiration in hydrological cycles influences the isotope of cistern water.
- End member model is used to study the recharge source of water cisterns.
- D-excess and TDS were used to classify three runoff mixing patterns.
- Seasonal isotopic response can reflect the recharge stability of water cisterns.

GRAPHICAL ABSTRACT

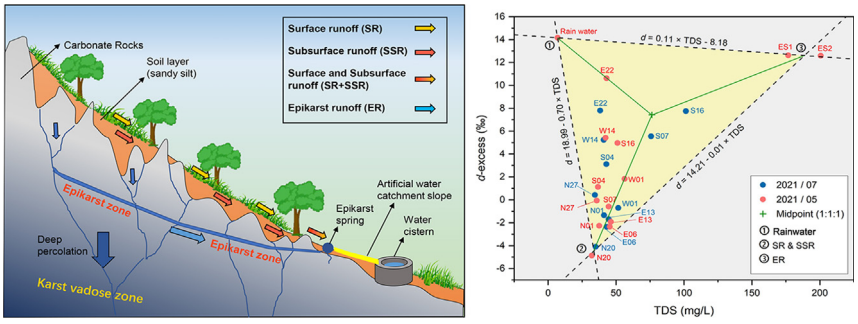

ARTICLE INFO

Editor: José Virgílio Cruz

Keywords:
Subsurface hydrological process
Stable hydrogen and oxygen isotopes
Rainwater harvesting project
Epikarst spring
Karst depression

ABSTRACT

Rainwater harvesting (RWH) projects in a decentralized way are significant measures to deal with the water scarcity dilemma in rural areas of the karst mountains in Southwest China at present. Due to the differences in cistern construction features and geomorphological positions, the water sources of cisterns were characterized by marked spatial variability, and the recharge stability of cisterns was strongly influenced by precipitation seasonality. Nevertheless, in hydrological processes on karst hillsides, the identification of different runoff types of RWH has not been sufficiently studied. The stable isotopes of hydrogen and oxygen of eleven cisterns and epikarst springs in subtropic cockpit karst landforms were monitored from 2020 to 2021 to investigate the runoff characteristics in RWH. Evaporative fractionation in different hydrological cycles is the predominant factor regulating the stable isotopic signature of cistern water. The results indicated that the typical roles that occurred in the recharge process contributed differently to water harvesting, with surface runoff (SR) and subsurface runoff (SSR) contributing much more than rainwater (RW) and epikarst runoff (ER). Three mixing patterns were proposed by end-member analysis in which SR + SSR, ER, and RW were three end members with indicators of isotopic value and the total dissolved solids (TDS). The recharge of SR + SSR was the predominated source, which contributed to 64% of the total water resources collected through RWH in the rainy season. In addition, the influence of various runoffs on the recharge stability of the cistern can be reflected by the multiple statistical analysis of isotopic fluctuation. Poor recharge stability is caused by excessive SR + SSR, whereas a higher percentage of ER and RW leads to better recharge stability. The applied method of hydrological process analysis is significant to the cistern water resources management in rural areas of the karst mountains.

* Corresponding author.
E-mail address: bmnxz@126.com (G. Jiang).

http://dx.doi.org/10.1016/j.scitotenv.2022.154924
Received 31 December 2021; Received in revised form 21 March 2022; Accepted 26 March 2022
Available online 29 March 2022

1. Introduction

Karst landscapes cover 15.2% of the global land area, and 16.5% of the world's population depends on karst water (Goldscheider et al., 2020). Seasonal water resource shortages have become an important factor restricting the development of local agriculture and other industries in rural areas of the karst mountains in Southwest China (Jiang et al., 2019; Yuan, 2014). The occurrence of extreme droughts can even threaten the drinking water security of humans and livestock. The formation of karst cracks and conduits has resulted in significant surface water leakage, which is the primary reason for water scarcity in this area (Qin et al., 2015; Williams, 2008). Rainwater harvesting (RWH) has been widely applied and extensively studied in recent years, especially in urban districts (Campisano et al., 2017; Feng et al., 2022; Li et al., 2021). The RWH project aims to reuse rainwater, mainly for irrigation, household, and municipal cleaning. In the karst mountains, the use of decentralized water cisterns or water tanks to store runoffs generated during rainfall is an important measure to address the problem of water scarcity. They are the only water source and cover all daily living and manufacturing. Most of the cisterns are built at the foot of the hillsides to collect more slope runoffs during rainfall. Some cisterns adjacent to epikarst springs can harvest spring water to improve collection efficiency (Jiang et al., 2019). As a result, the harvesting of runoffs generated by hydrological processes of karst slopes driven by rainfall is substantial for RWH in this region. Therefore, slope hydrological processes regulate the quantity and quality of water, apart from those using the rooftops as catchment surfaces.

Surface runoff (SR) at the atmosphere-soil interface, subsurface runoff (SSR) at the soil-epikarst interface, and epikarst runoff (ER) generally represented by epikarst springs are the three primary forms of runoff generated during slope hydrological processes of karst hillsides (Fu et al., 2015b). Due to the considerable heterogeneity in the distribution and thickness of soil layers on karst slopes, carbonate rocks can be immediately exposed on the surface, making the generation of continuous runoff in soil layers difficult (Cao et al., 2003). As a result of weathering and erosion, the soil-epikarst interface is commonly structured as “soil-filled grikes,” allowing SSR from the soil layer to drain down the slope at the interface after subsurface saturation areas in each grike connecting on a large scale, a theory known as “fill and spill” (Wang et al., 2020c). Surface and subsurface runoff generation coefficients are related to rainfall intensity, soil water content, soil distribution, topographic slope, infiltration coefficient of epikarst karst zone, and karst morphology (Fu et al., 2015a; Fu et al., 2015b; Uber et al., 2018; Wang et al., 2020c; Yan et al., 2018). SSR at the soil-epikarst interface infiltrates and recharges the underlying epikarst zone, the structure of which determines the dynamics of the water cycle in the soil-epikarst system (Perrin et al., 2003). Epikarst runoff is discharged as an epikarst spring if the rainfall threshold is satisfied (Jiang et al., 2008). Groundwater recharge processes are impacted by concentrated infiltration of fast flow through conduits and fissure in the subsurface soil layers, and that fast recharge processes aggravate the vulnerability of the groundwater environment (Hartmann et al., 2017; Hartmann et al., 2021; Jiang et al., 2015). The undulating epikarst zone and the heterogeneous and discontinuously distributed soil layers form a dual structure in the karst area, making it challenging to study and predict slope hydrological processes with multiple runoffs, thus resulting in difficulties determining the water source of cisterns dependent on slope hydrological processes.

Stable hydrogen and oxygen isotopes are widely applied in hydrogeology to analyze groundwater circulation and recharge mechanisms (Batista et al., 2018; Hao et al., 2019; Ma et al., 2017; Mao et al., 2021). In karst basins, hydrological functions, such as rainfall mixing, hydrological connection, and flow routes, can be identified by hydrogen and oxygen isotopes (Qiu et al., 2022; Wang et al., 2020b; Zhao et al., 2018). The flow characteristics of soil water on karst slopes are dominated by vertical piston flow at the soil-epikarst interface, as revealed by hydrogen and oxygen isotope signatures in previous studies (Liu et al., 2017; Zhang et al., 2021). The most significant factor determining isotope values is the variations in evapotranspiration through distinct water cycle paths (Hu et al., 2015). Evaporation of surface soil water varies the vertical distribution of hydrogen and oxygen isotopes, with isotope values at the surface layer tending to be positive, and this evaporation occurs primarily within a few millimeters of the surface soil (Gowing et al., 2006; Xu et al., 2018). As a result, SR has higher isotopic values than rainwater. Evaporative fractionation usually occurs at the vapor-liquid phase junction, resulting in heavier hydrogen and oxygen isotopes enrichment (Bao et al., 2008). For the water stored in the regular water cistern. Evaporative fractionation is the most significant factor determining the isotope values of water in the regular cisterns without covers. In addition, temperature also has a notable impact on the evaporative fractionation process under equilibrium circumstances (Kim and Lee, 2011).

End member mixing models are widely applied in hydrological systems to separate the contributions of different water sources (Lee and Krothe, 2001). Tracers in the models should be satisfied with the assumption that no chemical reactions occur throughout the mixing process, and the stable hydrogen and oxygen isotope is the most widely used indicator. This model could quantify the contribution of different recharge processes to groundwater, where the two end members are the average isotopic values of atmospheric precipitation in summer and winter (Mao et al., 2021; Solder and Beisner, 2020). In addition, previous researches have classified different runoff ratios using water chemistry indicators for end-member mixing analysis, such as Cl^- (Arbel et al., 2010), NO_3^- (Wang et al., 2020a), and Ca^{2+}/Sr^{2+} (Kang et al., 2011). Therefore, end members specified by different flow processes can determine mixing ratios in various hydrological circumstances where water mixing happens. In the hydrological process, SSR is produced by saturating the soil layer and circulating through the soil layer over a certain time. Therefore, theoretically, SSR has a higher TDS than SR. The isotopic values of SSR can be influenced by the effect of soil water evaporation. SR is more affected by slope vegetation withering and topsoil. Therefore, heavy isotopes are enriched in SSR and SR. TDS increases significantly due to the water-rock interaction with carbonate rocks after precipitation infiltrating into the epikarst zone. The isotope values are negative as the ER is not affected by evaporative fractionation. In summary, stable hydrogen and oxygen isotopes sampled in cisterns combined with water chemistry data can identify the variations in different recharge sources during the surface-subsurface hydrological processes on karst slopes. Related researches in the karst area mainly focus on improving harvesting efficiency and revealing the process of water quality deterioration (Chen et al., 2004; Jiang et al., 2019; Qin et al., 2015). However, not enough studies have attempted to analyze the slope hydrological processes involved in identifying different recharge sources of cisterns. The mixing mechanisms of runoffs generated in surface-subsurface hydrological processes in rainwater harvesting projects due to the heterogeneity of karst slopes were the main scientific issues of this paper.

There are multiple sources for a specific water cistern in different seasons, and the contribution percentage of every source depends on the amount and intensity of the rainfall. The challenge is to differentiate the runoffs of SR, SSR, and ER generated in the hydrological process on karst slopes. The construction features of water cisterns can determine the recharge sources in most instances. However, before runoffs enter cisterns, the mixing of diverse runoffs in the harvesting process is usually overlooked, especially for SSR and ER. The objectives of this study are (1) to clarify the cisterns' recharge sources and stabilities by analyzing isotope distribution and fluctuation of cistern water, rainwater and epikarst spring water, (2) to determine the mixing of runoffs in surface-subsurface hydrological processes by end-member analysis, and (3) to evaluate the water quantity and quality risks of the sampled cisterns. Furthermore, the research findings may contribute to more precise models for water cistern management in karst mountainous areas.

2. Materials and methods

2.1. Study area

The study area is in a small and remote village called Nonglei (24°31′14″N, 107°5′5″E), which belongs to Fengshan County, Hechi City,

Southwest China (Fig. 1A). Nonglei locates at the base of a karst depression, with a typical cockpit karst landform. The highest point on the north side of the depression is 929 m above sea level, and the lowest point in the center of the depression is 556 m (Fig. 1B). Fengshan County is in a subtropical monsoon area, near the southern foot of the Yunnan-Guizhou Plateau, with abundant rainfall, mild and humid weather. The average annual temperature is 19.4 °C, and the average annual rainfall is 1506 mm (1951–2013) (Liu et al., 2021). Precipitation is distributed unevenly throughout the year, with the rainfall amount from May to September accounts for 77% of the annual amount (Jiang et al., 2019). The strata in the study area are the Upper Carboniferous, and the lithology is medium-thick layered limestone with dolomite (Liu et al., 2021). With a thickness ranging from 0 to 1 m, the distribution of soil on slopes is uneven. The predominant soil texture is sandy silt. The vegetation coverage on the hillsides is more than 90%, based on the survey of UVA.

Nonglei village relies on RWH as its only source of water. The water cisterns are often constructed near the foot of the hill or in the middle and lower part of the slope, and they may receive a variety of runoff replenishment via the artificial water catchment surface. Fig. 2 depicts a basic pattern of a hillside cistern and represents the three forms of runoff and their corresponding circulation pathways. Most water cisterns follow this pattern, except for a minority that use the rooftop as a catchment surface to directly collect rainfall. The artificial water catchment surface at the junction of the water cistern and the slope surface is usually hardened by cement. Through this catchment surface, the mixed runoffs generated during the rainfall process and the epikarst springs could flow into the water cistern. The capacities of cisterns were generally between 200 and 600 m^3. Most of the cisterns were designed without cover. Steel meshes were used on some cisterns with trees nearby to cover leaves (E22, S04).

The edge of artificial catchment surfaces is usually covered with bedrock beneath the soil layer to improve engineering stability. As a result, SSR generated from the soil-epikarst interface can be collected in cisterns through the catchment surface. Although the collection efficiency of SR + SSR is high during rainy seasons, it is less effective in coping with seasonal water shortages. The possibility of collecting ER depends on the location of the epikarst springs and the engineering geology of the slope. The rainfall threshold of epikarst springs is smaller than slope runoff in the karst hillside, so it is more secure in dealing with seasonal water scarcity and has better water quality (Jiang et al., 2021; Wang et al., 2020c). Rainwater collection through rooftops is relatively rarely used due to the lower collection efficiency. Water cisterns for drinking purposes are equipped with filtration and purification systems to ensure that the water is safe to consume.

2.2. Sampling methods and field measurements

Water samples for hydrogen and oxygen isotope were collected from 11 cisterns in September 2020, January 2021, March 2021, May 2021, and July 2021. The locations of the sampling cisterns were shown in Fig. 1C. Table 1 described the geomorphological positions and the construction features of the 11 sampling cisterns. In the study area, based on architectural features, water cisterns can be divided into five categories: (1) artificial

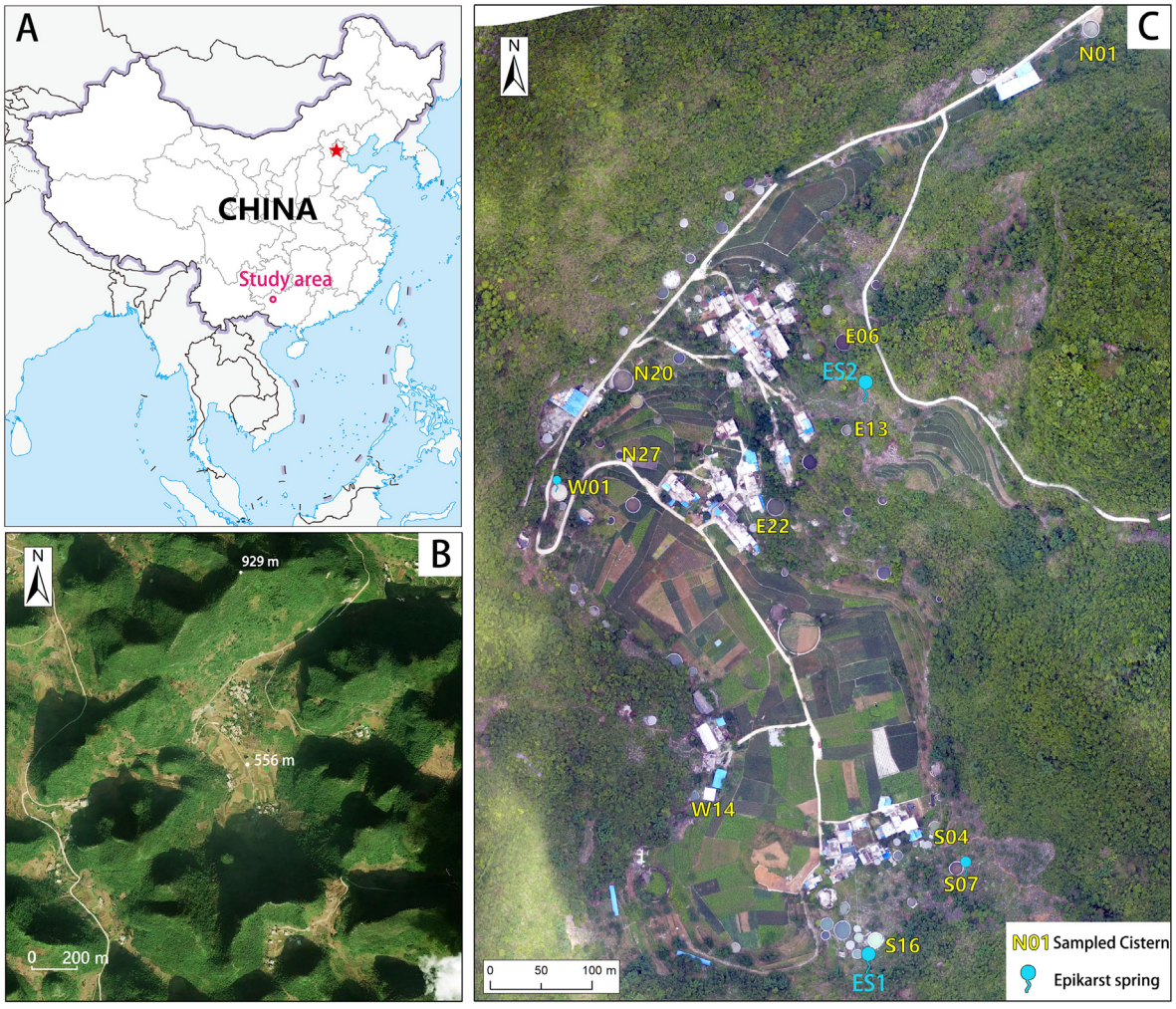

Fig. 1. A. Location of study area; B. Geomorphology map of the karst depression of Nonglei; C. Distribution of sampled cisterns and investigated epikarst springs.

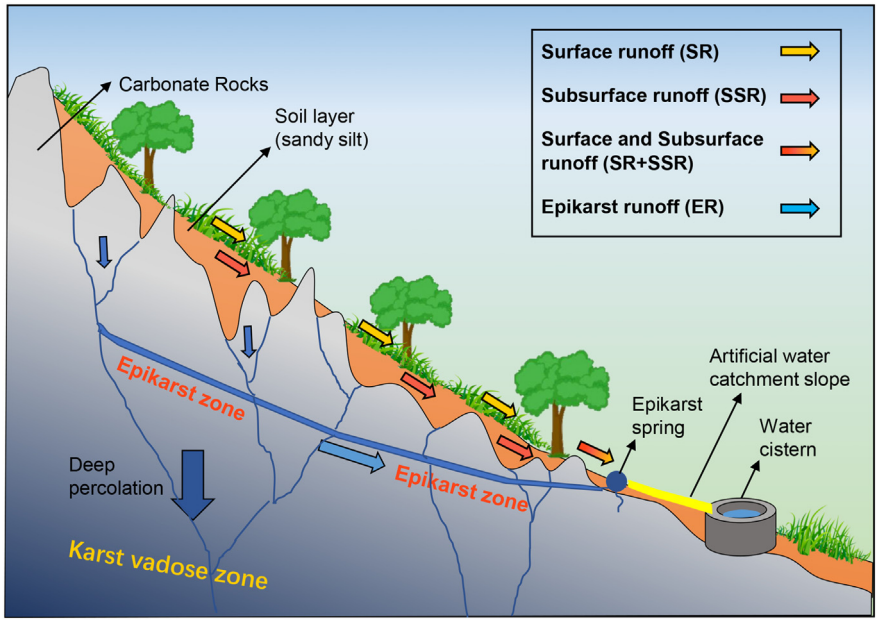

Fig. 2. Basic recharge pattern of the water cistern in karst mountainous areas.

water catchment slope, (2) artificial water catchment slope and epikarst spring, (3) epikarst spring and natural slope, (4) artificial water catchment slope and rooftop catchment, (5) rooftop catchment. The 11 water cisterns cover these five types. For each water cistern in Table 1, five water samples were collected in five different months. Two epikarst springs (ES1 and ES2) were sampled once in May 2021. ES1 was around the S16 cistern at the depression's southern slope, and ES2 was located above the E13 cistern near an old and damaged cistern. Rainwater samples were collected cumulatively in May 2021 and September 2020 separately. A funnel with a plastic table tennis ball in it was attached to the mouth of the sample bottle to prevent evaporation. TDS values of the 11 cisterns were tested in situ by the Ponsel multiparameter water quality analyzer (France) during cistern sampling in May and July 2021. Therefore, 22 water samples from the 11 cisterns had isotopic and TDS values of two periods in rainy season.

Water samples were collected using 30 mL high-density polyethylene bottles devoid of air bubbles to prevent isotope evaporative fractionation. The stable isotopic compositions were measured by high-precision laser spectroscopy (LGR LWIA-24d, USA) at the Key Laboratory of Karst Dynamics, Ministry of Natural Resources. The δ^2H and $\delta^{18}O$ values were reported relative to the VSMOW (Vienna Standard Mean Ocean Water) in per mil (‰). The measurement precision for δ^2H and $\delta^{18}O$ was 0.5 and 0.05‰, respectively. Precipitation and temperature data were obtained from China Meteorological Data Network (http://data.cma.cn) with an accuracy of the daily value. Origin 2021, Matlab 2016, SPSS 19, and ArcGIS 10.2 were applied for data analysis and graphing.

Table 1
Geomorphological positions and construction features of the eleven cisterns.

Cistern number	Geomorphological positions	Construction features
E06	Middle of slope	Artificial water catchment slope
E13	Middle of slope	Artificial water catchment slope
N20	Foot of slope	Artificial water catchment slope
S04	Lower part of slope	Artificial water catchment slope
N01	Foot of slope	Artificial water catchment slope and epikarst spring
W01	Foot of slope	Artificial water catchment slope and epikarst spring
S07	Middle of slope	Artificial water catchment slope and epikarst spring
S16	Lower part of slope	Epikarst spring and natural slope
N27	Foot of slope	Artificial water catchment slope and rooftop catchment
E22	Foot of slope	Rooftop catchment
W14	Foot of slope	Rooftop catchment

2.3. Deuterium excess analysis

Dansgaard (1964) proposed and defined the deuterium excess parameter as:

$$d\text{-excess} = \delta^2H - 8 \times \delta^{18}O \quad (1)$$

The *d*-excess value is sensitive to non-equilibrium fractionation processes driven by different diffusion rates of aqueous isotopes during evaporation (Masiol et al., 2021; Pfahl and Sodemann, 2014). D-excess can be reflected by differences in isotope exchange along with different water cycles from the same source. Strong evaporative fractionation can lead to heavy isotope enrichment, and the *d*-excess value tends to decrease (Hu et al., 2018; Sprenger et al., 2016).

2.4. End member mixing analysis

There are three sources mixed in the recharge process of the water cistern: slope runoff (SR, SSR), rainwater (RW), and epikarst runoff (ER). The *d*-excess and TDS value were tracers in the end-member mixing analysis. The seasonal variation in rainwater isotopes is high due to the different sources of water vapor in different seasons. The recharge of the water cisterns mainly occurred during the rainy season, so the water samples of the selected end-members were collected in the rainy season. Rainwater in the rainy season was collected directly with sample bottles as the RW end-member. ER end-members were selected from the two largest epikarst springs in the depression (ES1 and ES2). The N20 water cistern serves as the end-member of the SR + SSR because it has the largest catchment slope area and relies on the road above to expand the catchment area. The E06 water cistern is similar to the N20 water cistern in that it also relies on the road surface to extend the catchment area. However, it is affected by the undulations of the road surface and has a lower harvesting efficiency than the N20.

According to the law of mass conservation, the contribution of each source can be calculated by solving the following equations:

$$C_dV_m = C_{dS}V_S + C_{dR}V_R + C_{dE}V_E \quad (2)$$

$$C_TV_m = C_{TS}V_S + C_{TR}V_R + C_{TE}V_E \quad (3)$$

$$V_m = V_S + V_R + V_E \quad (4)$$

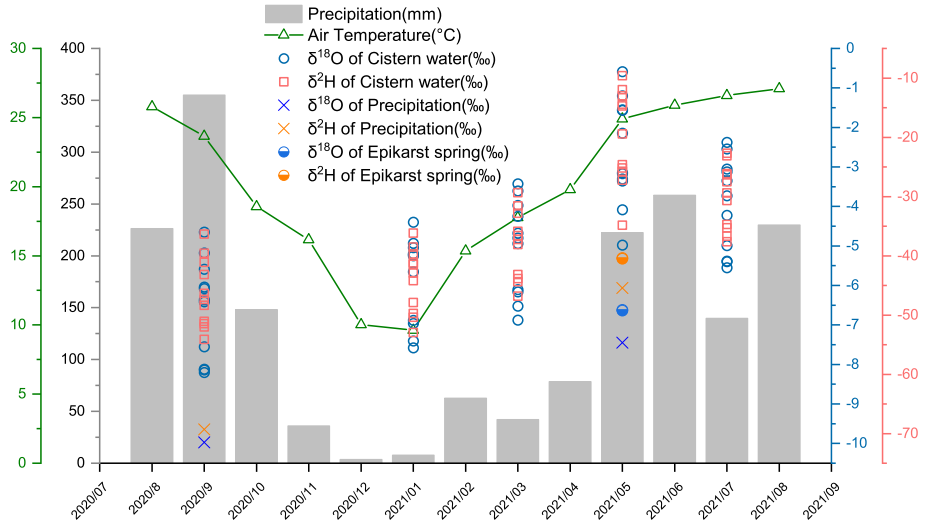

Fig. 3. Seasonal variations of the δ^2H and $\delta^{18}O$.

where V_m is the volume after mixing, V_S, V_R, V_E are the volumes of SR + SSR, RW, and ER, respectively; C_d is the *d*-excess value after mixing, C_{dS}, C_{dR}, C_{dE} are the *d*-excess values of SR + SSR, RW, and ER, respectively; C_T is the TDS value after mixing, C_{TS}, C_{TR}, C_{TE} are the TDS values of SR + SSR, RW, and ER, respectively. By solving the linear equations, the ratio of each source in the mixing process can be derived: $\frac{V_S}{V_m}$, $\frac{V_R}{V_m}$, $\frac{V_E}{V_m}$. The calculation process was performed in Matlab.

2.5. Multi-temporal hierarchical clustering analysis

The values of $\delta^{18}O$ and *d*-excess, which are sensitive to the typical response of evaporative fractionation, are selected as variables in hierarchical clustering analysis (HCA). The analysis was performed with the Ward clustering algorithm and Euclidean distance. The multi-temporal data from five different periods can reveal the seasonal variation characteristics. The clustering process was performed in SPSS.

3. Results

Fig. 3 depicted the variations on the δ^2H and $\delta^{18}O$ of water in cisterns in the study area. The descriptive statistical analysis by month was illustrated in Table 2. The isotope values in the water cisterns sampled in different months varied significantly. The trend of the average values of δ^2H and $\delta^{18}O$ from the largest to the smallest was: May–July-March-January-September. The heavier isotopes were most enriched in May and least enriched in September. The minimum isotopic values of the cisterns in autumn were consistent with the trend of precipitation isotopes and were attributable to the extremely heavy rainfall in September 2020 with lower isotopic values, which were −69.28‰ (δ^2H) and −9.79‰ ($\delta^{18}O$). The standard deviation was highest in May, lowest in January and September, and the range was also highest in May (Table 2). The standard deviation and range reflected the significant variations in the recharge sources in the wet and dry periods. Table 3 depicted the descriptive statistical analysis classified by water cisterns. The average value of the δ^2H and $\delta^{18}O$ in Table 3 represented the difference of recharge source between cisterns in the hydrological process on karst slopes. The mean values of δ^2H and $\delta^{18}O$ of E06, N20, and E13 were relatively positive, which were −27.30‰, −30.66‰, −33.53‰ (δ^2H) and −3.24‰, −3.51‰, −4.09‰ ($\delta^{18}O$), respectively, showing that their recharge source was primarily heavy isotope-enriched runoff. The mean values of δ^2H and $\delta^{18}O$ of E22, and S16 were relatively negative, which were −40.18‰, −41.64‰ (δ^2H) and −6.15‰, −6.00‰ ($\delta^{18}O$), respectively. Water cisterns with larger standard deviation and range values (S07, W01, N20, E22) had a greater variation in recharge composition from different seasons, whereas water cisterns with smaller standard deviation and range values (S04, N27, E06) had a more consistent and stable source of recharge (Table 3). Table 4 presented the TDS values during the rainy season (May and July), with epikarst springs characterizing the greatest TDS of 200.6 mg/L and rainwater characterizing the lowest TDS of 6.93 mg/L. The TDS values of the water cisterns were all in the range of rainfall and epikarst springs, indicating that the multiple recharge sources were mixed. The TDS values of the water cisterns ranged from 32.19 mg/L to 101.4 mg/L, revealing that the mixing ratios varied widely.

The plot of δ^2H versus $\delta^{18}O$ for cisterns and epikarst springs samples was depicted in Fig. 4. The stable isotopes exhibited significant seasonal variations, enriched in the rainy season while depleted in the heavy isotopes in the dry season. The GMWL was the global atmospheric precipitation line (Craig, 1961), and the LMWL was the local atmospheric precipitation line (2017 to 2018) established by Wang et al. (2020b) in Huanjiang County, Hechi City. The slope of the LMWL was almost equal

Table 2
Descriptive statistical analysis of isotopes for different months.

Month	Range		Mean value		Standard deviation	
	δ^2H (‰)	$\delta^{18}O$ (‰)	δ^2H (‰)	$\delta^{18}O$ (‰)	δ^2H (‰)	$\delta^{18}O$ (‰)
2020/09	17.77	3.55	−46.43	−6.57	5.74	1.25
2021/01	16.76	3.18	−44.08	−5.86	5.42	1.12
2021/03	17.48	3.45	−38.15	−5.03	5.74	1.21
2021/05	25.26	4.39	−20.06	−2.64	7.97	1.34
2021/07	14.94	3.18	−30.00	−3.97	5.38	1.19

Table 3
Descriptive statistical analysis of isotopes for each cistern.

Cistern number	Range		Mean value		Standard deviation	
	δ^2H (‰)	$\delta^{18}O$ (‰)	δ^2H (‰)	$\delta^{18}O$ (‰)	δ^2H (‰)	$\delta^{18}O$ (‰)
E06	24.41	3.45	−27.30	−3.24	10.27	1.42
E13	33.92	4.80	−33.53	−4.09	13.54	1.87
E22	39.40	4.95	−40.18	−6.15	16.15	1.97
N01	27.93	4.27	−35.08	−4.43	11.87	1.77
N20	36.76	5.45	−30.66	−3.51	14.73	2.13
N27	16.00	2.45	−34.81	−4.48	7.21	1.03
S04	17.43	2.72	−34.92	−4.76	6.82	1.03
S07	38.47	6.65	−34.66	−4.83	14.10	2.41
S16	15.52	2.43	−41.64	−6.00	6.67	1.08
W01	27.37	4.83	−39.02	−5.57	12.29	2.17
W14	23.81	3.47	−41.40	−5.93	10.21	1.40

Table 4
TDS values during rainy season (May and July).

Cistern number	TDS (mg/L)	
	2021/07	2021/05
E06	43.06	45.32
E13	44.53	46.15
E22	38.26	42.99
N01	41.2	37.65
N20	35.05	32.19
N27	34.42	35.77
S04	42.91	36.77
S07	75.83	44.59
S16	101.4	51.04
W01	51.6	56.31
W14	40.88	42.3
Precipitation	No data	6.93
ES1	No data	176.7
ES2	No data	200.6

to the GMWL, with a slightly larger intercept than the GMWL. As shown in Fig. 4, red points represented the rainy season, and green points represented the dry season. The red evaporation line (EL) in the rainy season was above the EL in the dry season because of the significant differences in evaporative fractionation between seasons. Most of the cistern samples were distributed under the GMWL and the LMWL, and isotopic values were characterized with obvious seasonal zonation.

4. Discussion

4.1. Stable hydrogen-oxygen isotope and d-excess analysis

Previous research showed that precipitation isotopes in the Hechi region had maximal values in the winter and spring and minimal values in the summer and autumn (Wang et al., 2020b). The minimums occurred during the rainy season commonly (Guo et al., 2015). As exhibited in Fig. 3, the trend of cisterns isotopes from winter to spring was the inverse pattern of the precipitation isotopes due to the strong effect of evaporative fractionation. The intersection of the EL and LMWL, which was surrounded by the cistern samples in September, could represent the isotopic signatures not significantly affected by evaporation (Huang et al., 2017; Mao et al., 2021).

Fig. 5 showed the fluctuation curves of δ^2H and $\delta^{18}O$ by month. The general trend in isotope values was decreasing in the order of cisterns displayed in Fig. 5. N20 and E06 are water cisterns with roadway

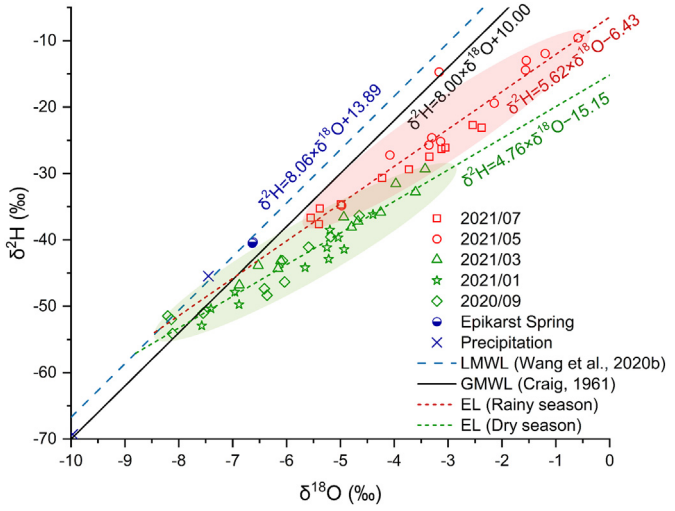

Fig. 4. Plot of δ^2H versus $\delta^{18}O$ for cisterns, epikarst springs, and precipitation samples. Red areas present rainy season samples, green areas present dry season samples. EL stands for Evaporation line.

catchment surfaces, which represented higher proportions of slope runoff. The isotope values of rainwater and epikarst springs collected in the rainy season tended to be negative. The cisterns in the light-yellow areas (E06, N27, and S04) exhibited a clear contraction characteristic, which corresponded to the smaller range value of isotopes in Table 3. This indicated a more consistent source of recharge and less seasonal variance. The water cisterns in light-grey areas (S07 and S16) showed a clear difference in recharge sources. S07 revealed isotopic anomalies in July 2021 and September 2020. According to the field survey, many mulberry trees were planted for sericulture on the slope above S07, and agricultural activities on the slope resulted in an unstable source of runoff (Peng and Wang, 2012). The isotopic abnormality exhibited in the S16 cistern was in September 2020. According to the field interviews, agricultural activities caused localized vegetation destruction on the slope above S16 and extremely heavy rainfall in September 2020 flushed some soil into the cistern, leading to the enrichment of heavy isotopes. The local multi-year average rainfall in September was 118 mm, while in 2020 there was 355 mm of precipitation occurred in September (Jiang et al., 2019). This phenomenon reflected the soil erosion process under extreme rainfall conditions in karst mountainous areas (Yan et al., 2018). To better highlight the seasonal variation features of cistern recharge sources, the third quartile of standard deviation (Q_3) of $\delta^{18}O$ in Table 3 was calculated with the result of 2.05. S07, W01, and N20 were cisterns with standard deviations bigger than Q_3, indicating poor recharge stability.

Plots of *d*-excess by month were shown in Fig. 6. N20 and E06 were typical SR + SSR recharged cisterns, characterizing the heaviest isotopic values in the rainy season. The *d*-excess value of the black dashed line was 0‰, the *d*-excess value of the fuchsia dashed line was 5‰, and the *d*-excess value of the yellow dashed line was −5‰. The samples, which were mainly recharged by SR + SSR, were relatively close to the yellow line, whereas the samples recharged by ER or RW were closer to the fuchsia line. The SSR was generated at the soil-epikarst interface, where the preferential flow was dominated in the process of infiltration and saturation in soil-filled grikes (Fu et al., 2016; Wang et al., 2020c). The enrichment of heavy isotopes in soil water was due to the evaporative fractionation of the topsoil. In the rainy season, the mixing of abundant rainwater and heavy isotopes enriched soil water led to $\delta^{18}O$ enrichment of SSR at the soil-epikarst interface (Zhang et al., 2021). During the recharge of SSR, a decrease in *d*-excess values of cistern water was caused by secondary evaporation processes (Batista et al., 2018). Compared to SR, SSR passed through a saturation process in the soil layer and had heavier isotope values. The hydrological process of SR was similar to the harvesting process of rainwater through the rooftops which were covered with moss and weeds due to atmospheric deposition, dense vegetation, and warm, humid climatic conditions. As a result, the *d*-excess values of E22 (RW) and W14 (SR) were all around the fuchsia line. For the hydrological process of the epikarst zone, rainfall could recharge the epikarst zone through fissures and conduits rapidly, the evaporative fractionation was much weaker than soil water. Moreover, the water-rock interaction in the epikarst zone could result in lower $\delta^{18}O$ values (Guo et al., 2018; Zhou et al., 2017). Therefore, the water cisterns recharged by epikarst springs had a higher *d*-excess value, such as S16.

4.2. Characterizations of recharge sources in the rainy season

The water in cisterns was mixed by four types of runoffs during the harvesting process, namely SR, SSR, ER, and RW. Soil layers on the slopes of karst depression areas are thin and unevenly distributed, and soil moisture content varies considerably. According to the mechanism of SSR generation during hydrological processes on karst slopes, soil water, which is affected by evaporation, accumulates and influences SSR. As a result, the isotope values of SSR were relatively positive. Atmospheric precipitation is the source of recharge for regional runoffs. The isotope values of RW were relatively negative. The isotopic values of SR are intermediate between the two. TDS value was applied to identify the hydrological processes of ER, as epikarst springs were characterized with a higher TDS value than other

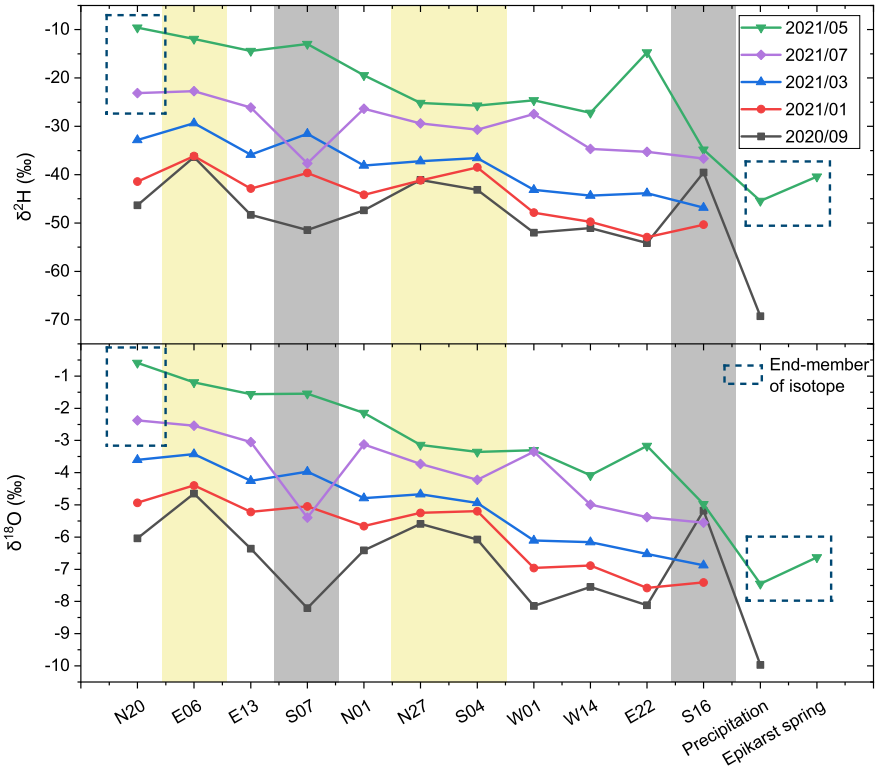

Fig. 5. Fluctuation curves of δ^2H and $\delta^{18}O$ by month.

forms of runoff. The mixing of three recharge sources was plotted based on the TDS and isotope values in May and July 2021 (Fig. 7). The mixing plot in May and July was significantly representative since the major recharging process occurred during the rainy season and it was difficult to generate much efficient recharge during the dry season. A thorough distinction between SSR and SR was hard to determine just on cistern water sampling analysis, which could only indicate the mixing extent of them. For this reason, there were three end members in the mixing process. As shown in Fig. 7, RW, SR + SSR, ER were located at the three vertices as three end members. The first end member was defined by rainwater samples. The second end member for SR + SSR was defined by cistern N20, whereas the third end member for ER was assigned by the mean values of ES1 and ES2. Rainwater had the smallest TDS values and the most negative isotope values, while epikarst springs were characterized with the highest TDS values and relatively negative isotope values. In contrast to them, SSR enriched heavier isotopes. There was a big epikarst spring (ES1) channeled into cistern S16 (Fig. 1C). As a result, S16 was significantly affected by ER. The cistern of E22, which was characterized as a rooftop catchment surface, was rainwater sourced.

The sample points were centered on the second end member with two "V" shaped branches, according to the data distribution trends exhibited in Fig. 7. Three types of mixing patterns (A, B, and C) were classified based on the end-member mixing analysis. Patterns A, which consists primarily of SR + SSR with a small quantity of RW and ER, covered the majority of sample points and was distributed around the second end member. Patterns B was distributed between the first and the second end member and relatively close to the first end member, which indicated a mixture dominated by RW and SR for the water cisterns that were not sourced from rooftops only. The closer to the first end member, the relatively higher the proportion of RW in it. Taking cistern W14 as an example, the contributions of RW and SR were relatively high in W14, which was built with a rooftop catchment and a small-scale catchment surface on a slope. Samples of pattern C were distributed in the area around the third between the second and the third end members, with a distinct ER mixing. As shown in Fig. 1C, cisterns of S16, S07, and W01 were all channeled by epikarst springs, which were affected by ER to some extent. It was worth noting that E13 and E06 were located to the right of the midpoint line in Fig. 7, indicating that they were influenced by a small portion of ER. Therefore, in the absence of significant epikarst springs, some epikarst runoff is still recharged as seepage from the soil-epikarst interface, mixing with SSR before flowing into cisterns.

Fig. 8 showed the mixing ratios of the three end members in the rainy season, with SR + SSR being the predominant recharge type, accounting for 64% of the total water resources in the sampled water cisterns. Although ER accounted for the smallest share, some epikarst springs recharged cisterns could collect spring water accumulatively in the absence of rainfall, which had great significance on water quality, as water quality deteriorated over time in cisterns (Jiang et al., 2019). The calculations revealed that the sources of some cisterns varied significantly between May and July, the reason was that the proportion of different runoffs generated varied with rainfall amount and intensity and that the TDS value of the epikarst springs fluctuated in the process of precipitation (Jiang et al., 2008; Wang et al., 2020c). For a precise mixing pattern study, more samples and longer-term monitoring were required. Only a basic model for mixing categorization was offered in this paper. The demographic composition of residents and the structure of the agricultural industry were comparable, according to the site survey, as were the per capita water requirements for residential and agricultural output. The construction volume of the water cistern was also determined by the number of permanent residents served. Accordingly, the water use strategies for each of the sampled cisterns were relatively similar. As a result, while the variations in evaporative fractionation owing to lengthy durations of water storage in a specific water cistern could not be ruled out and were prone to certain calculation errors, the differences in hydrological processes could still be reflected through the water samples in cisterns to some extent.

4.3. Seasonal scale recharge stability analysis

According to the previous conclusions, water cisterns of S07, W01, and N20 had poor recharge stability, which was derived from the standard

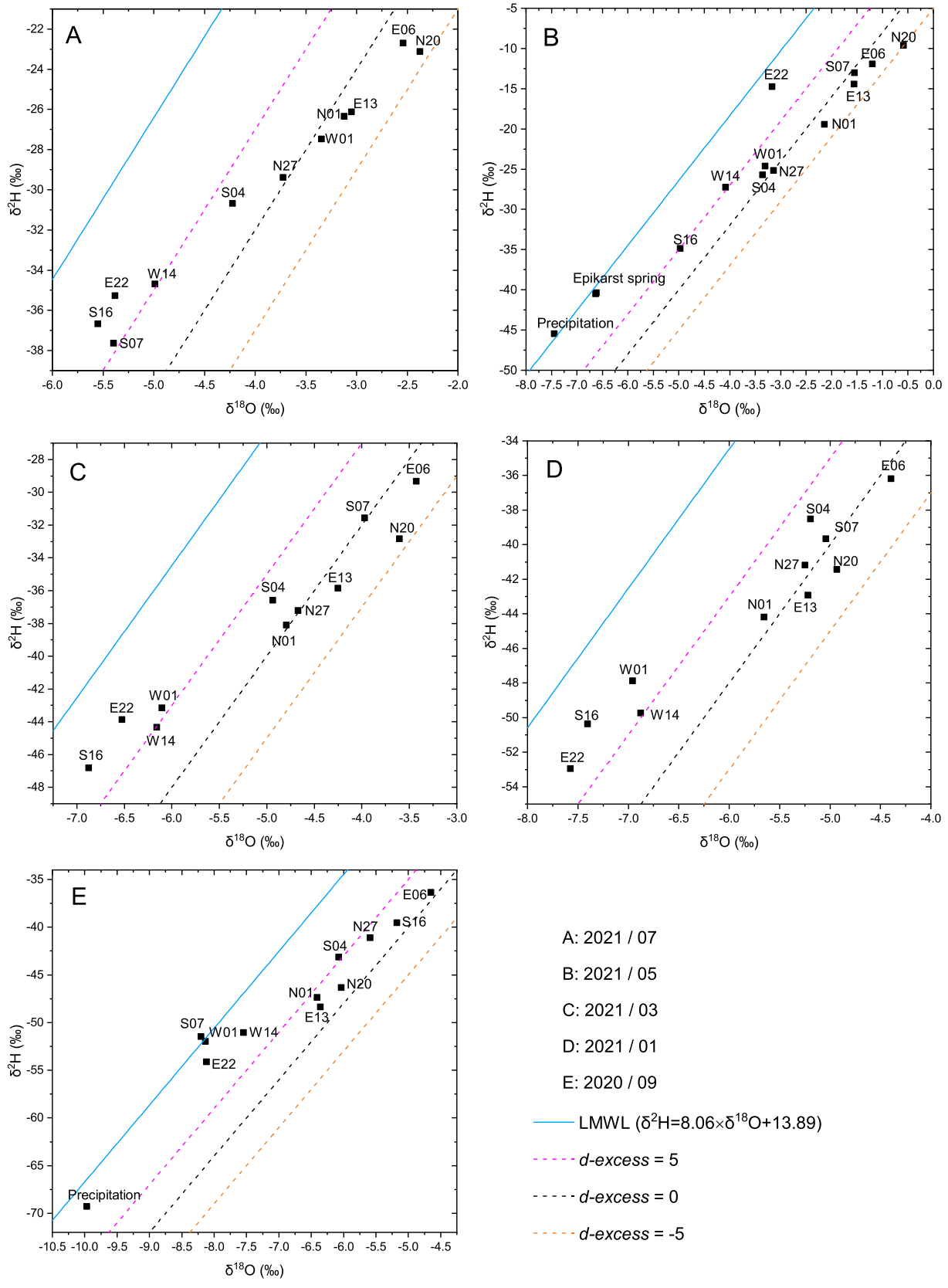

Fig. 6. Plot of δ^2H versus $\delta^{18}O$ and the *d*-excess values by month.

deviation statistics. Although this result reflected the overall trend, it did not account for the variations for each cistern on a seasonal scale. In order to elucidate the seasonal recharge variation, five hierarchical cluster analyses based on isotope data from the eleven water cisterns in various months were conducted. A distance between clusters of 10 was selected, with all cistern samples falling into two clusters each month. The significant

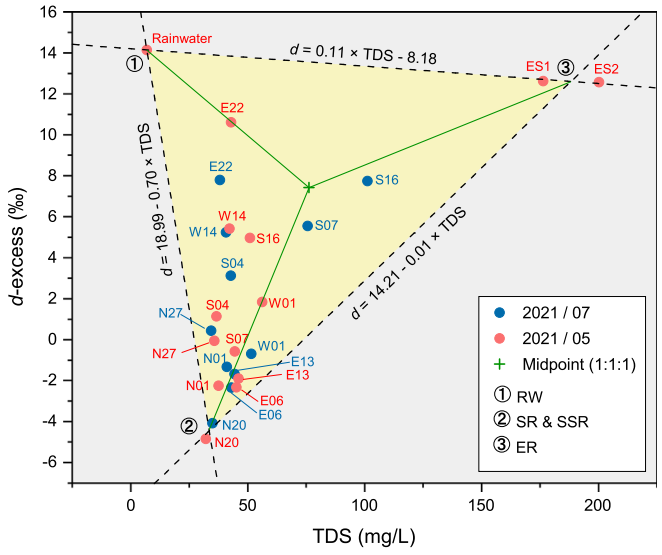

Fig. 7. Mixing of the three recharge sources during rainy season.

difference between the two clusters, according to the HCA, was whether they were impacted by SSR. The mixing with soil water exhibited characteristics that were clearly influenced by evaporative fractionation (Hu et al., 2015). Table 5 summarized the HCA results. Cluster 1 (C1) indicated little or a small proportion of SR + SSR mixing, with ER or RW predominated. Cluster 2 (C2) indicated a large proportion of SR + SSR mixing. Without the TDS indicator, ER and RW dominated cisterns would be classified in the same cluster. However, the cisterns that collected rainwater directly were easily distinguishable from construction features, making this method viable.

E22 and W14 were consistently in cluster 1 according to Table 5. Fig. 7 showed that they were RW dominated cisterns, both of which had similar

Table 5
Multi-temporal hierarchical clustering analysis.

Cistern number	2021/07	2021/05	2021/03	2021/01	2020/09
N20	C2	C2	C2	C2	C2
E06	C2	C2	C2	C2	C2
E13	C2	C2	C2	C2	C2
S07	**C1**	C2	C2	C2	**C1**
N01	C2	C2	C2	C2	C2
N27	C2	C2	C2	C2	C2
S04	**C1**	C2	**C1**	C2	C2
W01	C2	C2	**C1**	**C1**	**C1**
W14	**C1**	**C1**	**C1**	**C1**	**C1**
E22	**C1**	**C1**	**C1**	**C1**	**C1**
S16	**C1**	**C1**	**C1**	**C1**	C2

Note: C1 indicated cluster 1 (light blue) and C2 indicated cluster 2 (light yellow).

recharging processes and were characterized with good stability. For S16, epikarst spring (ES1) was the major source, thus characterizing good recharge stability in most instances. W01 was in cluster 1 during the dry

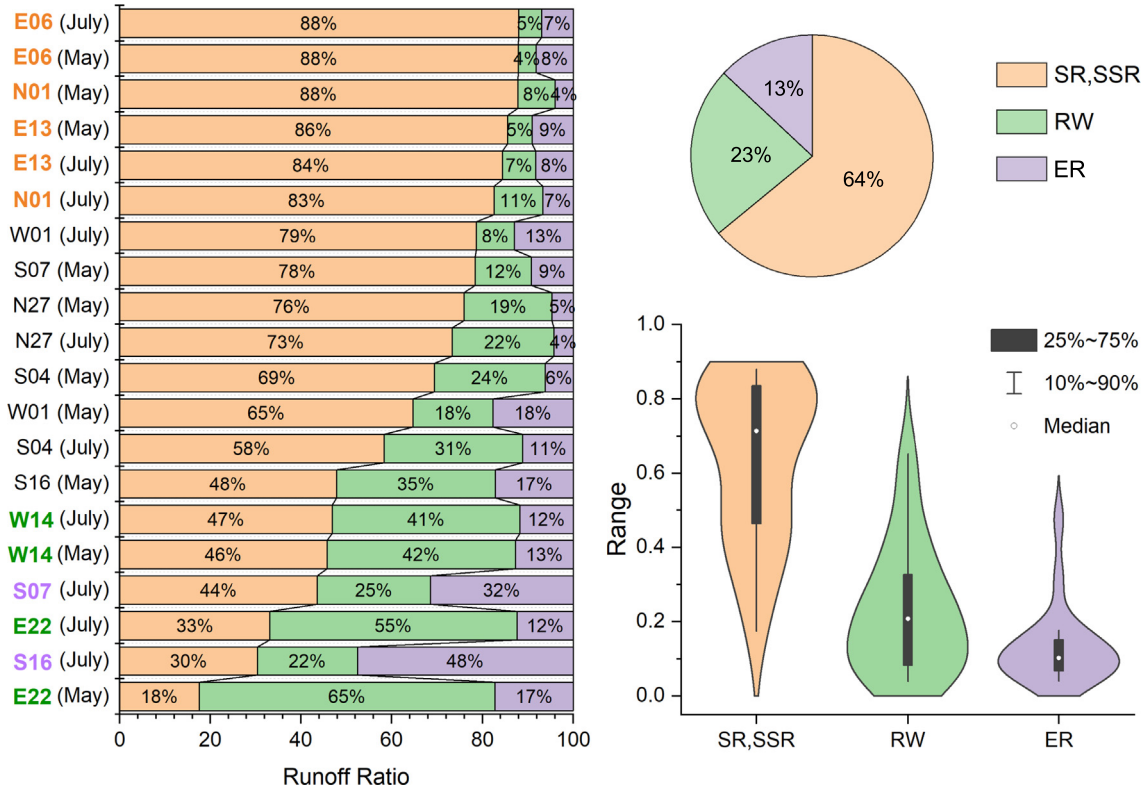

Fig. 8. Mixing ratios for each cistern in the rainy season.

season and cluster 2 during the rainy season. It was mainly recharged by a small epikarst spring and runoffs through the artificial water catchment slope above it (Fig. 1C). There was less influence from the SR + SSR mixing above the catchment during the dry season, but more influence during the rainy season, when recharge stability was poor. The N27 cistern, which included a rooftop catchment as well as a slope catchment, was consistently in cluster 2, indicating that SR + SSR was predominant and the recharge was relatively stable. S04 was in cluster 1 in March and July, indicating that it was mostly RW at the time, while cluster 2 in other months, revealing the dominance of SR + SSR and the poor recharge stability. E06 and E13 were relatively similar in terms of construction and both in cluster 2, indicating that their recharge processes were also relatively similar between months. N20 was in cluster 2 but had a higher statistical variance value, which was probably due to the fact that the catchment surface was adjacent to the road (Fig. 1C). Under the influence of human activities, the isotopes fluctuated considerably. N01 was in cluster 2, dominated by SR + SSR. There was a mixture of a small amount of epikarst spring in S07. Because of the considerable rainfall and spring flow in these months, S07 was classified as cluster 1 in July and September. The slope above S07 was covered with crops such as mulberry and maize and was subject to high levels of soil erosion due to agricultural activities, leading to unstable isotope values and poor water quality. In summary, for cisterns built with multiple collection routes, excessive SR + SSR often generated poor stability, but a higher percentage of ER and RW usually led to better stability, in most cases.

4.4. Management strategies and advice for different water cisterns in rainy season

SR + SSR is the primary source of water for cisterns in RWH. Despite the guaranteed amount of water, they are vulnerable to water quality risks. There is a need to focus on water quality monitoring from the perspective of drinking water safety. During the rainy season, when there is enough recharge, water cisterns should be cleaned at least once a year. The cisterns mainly sourced by ER have better water quality and quantity, but they are restricted by the location of the epikarst spring, making them difficult to replicate on a large scale. The cisterns with RW as the main source have better water quality, but the quantity is generally restricted by the size of the rooftop. In the case of E22, the cistern was built with pipes linking the rooftops of several nearby houses to ensure water collecting efficiency, but there was still a shortage of water in the dry season according to the visit. To avoid the possibility of contamination from excessive human activity, it is critical to guarantee the purity of the catchment surface and the environment of the slope above for water cisterns where SR + SSR is the primary source of recharge. Water quality safety issues caused by extreme rainstorms and water scarcity caused by extreme droughts must be considered.

However, some limitations and uncertainties should be noted. The hydrological processes during the dry season were not included in the discussion. The little renewal rate of the water in cisterns during the dry season made it difficult to calculate the runoff mixing ratio and could only reflect the trends in recharge. This limitation could be addressed in future research with observations of event rainfall. The main uncertainty in this study was the local heterogeneity of the karst medium. The cumulative collection of one rainwater sample in a month also brought some uncertainties in sampling and testing.

5. Conclusion

In the RWH of subtropical cockpit karst landforms, the analysis of stable hydrogen and oxygen isotopes revealed that the recharge sources consisting of SR + SSR, ER, and RW differed significantly in ratios. End member mixing analysis indicated that there were three mixing patterns in the recharge process in the rainy season: Patterns A covered the majority of cisterns characterized by SR + SSR dominated mixing process (N20, E06, N01, E13, N27, S04); Patterns B was dominated by RW and SR (E22, W14); Pattern C was characterized by a distinct ER mixing (S16, S07, W01). The recharge of SR + SSR was the predominated source, which contributed to 64% of the total water resources collected through RWH in the rainy season. The analysis of seasonal scale recharge stability by HCA showed that poor stability was usually caused by excessive SR + SSR for the cisterns mixed with multiple runoffs, whereas a higher percentage of ER and RW often led to better stability. The applied method of analyzing the surface-subsurface hydrological process of RWH is significant to the cistern water resource management in rural areas of the karst mountains.

CRediT authorship contribution statement

Fan Liu: Conceptualization, Methodology, Software, Writing - original draft, Investigation. **Guanghui Jiang:** Investigation, Writing - review & editing, Funding acquisition. **Guangcai Wang:** Supervision, Writing - review & editing. **Fang Guo:** Resources, Investigation, Visualization. **Jia Wang:** Writing - review & editing. **Qigang Wang:** Investigation. **Jie Shi:** Investigation. **Jingyi Cai:** Writing - review & editing. **Min Wang**: Supervision, Resources.

Declaration of competing interest

The authors declare that they have no known competing financial interests or personal relationships that could have appeared to influence the work reported in this paper.

Acknowledgments

This study was financially supported by the National Natural Science Foundation of China (42172287), the Guangxi Natural Science Foundation of China (2020GXNSFDA238013), and the Chinese Academy of Geological Sciences Research Fund (2020019). The authors thank Zhijie Li and Liqiong Wei for the assistance with sampling. The authors thank Dr. Shi Yu, Dr. Yanqing Li and Xujuan Huang for their help of data preparation. The authors thank Dr. Jianjun Yin and Prof. Zheming Shi for their thoughtful comments and suggestions.

References

Arbel, Y., Greenbaum, N., Lange, J., Inbar, M., 2010. Infiltration processes and flow rates in developed karst vadose zone using tracers in cave drips. Earth Surf. Process. Landf. 35, 1682–1693. https://doi.org/10.1002/esp.2010.

Bao, W., Hu, H., Wang, T., Zhai, S., 2008. Experimental study on the fractionation mechanism of hydrogen and oxygen stable isotopes in evaporation from water surface of evaporation pans. Adv. Water Sci. 19, 780–785.

Batista, L.V., Gastmans, D., Sánchez-Murillo, R., Farinha, B.S., dos Santos, S.M.R., Kiang, C.H., 2018. Groundwater and surface water connectivity within the recharge area of Guarani aquifer system during El Niño 2014–2016. Hydrol. Process. 32, 2483–2495. https://doi.org/10.1002/hyp.13211.

Campisano, A., Butler, D., Ward, S., Burns, M.J., Friedler, E., DeBusk, K., Fisher-Jeffes, L.N., Ghisi, E., Rahman, A., Furumai, H., Han, M., 2017. Urban rainwater harvesting systems: research, implementation and future perspectives. Water Res. 115, 195–209. https://doi.org/10.1016/j.watres.2017.02.056.

Cao, J., Yuan, D., Pan, G., 2003. Some soil features in karst ecosystem. Adv. Earth Sci. 18, 37–44.

Chen, Z., Wang, H., Chen, M., 2004. Current status and strategy of rainwater accumulation project in southwestern karst mountain area. China Water & Wastewater 9, 31–33.

Craig, H., 1961. Isotopic variations in meteoric waters. Science 133, 1702–1703.

Dansgaard, W., 1964. Stable isotopes in precipitation. Tellus 16, 436–468. https://doi.org/10.3402/tellusa.v16i4.8993.

Feng, W., Liu, Y., Gao, L., 2022. Stormwater treatment for reuse: current practice and future development - a review. J. Environ. Manag. 301, 113830. https://doi.org/10.1016/j.jenvman.2021.113830.

Fu, T., Chen, H., Zhang, W., Nie, Y., Gao, P., Wang, K., 2015a. Spatial variability of surface soil saturated hydraulic conductivity in a small karst catchment of southwest China. Environ. Earth Sci. 74, 2381–2391. https://doi.org/10.1007/s12665-015-4238-5.

Fu, Z., Chen, H., Xu, Q., Jia, J., Wang, S., Wang, K., 2016. Role of epikarst in near-surface hydrological processes in a soil mantled subtropical dolomite karst slope: implications of field rainfall simulation experiments. Hydrol. Process. 30, 795–811. https://doi.org/10.1002/hyp.10650.

Fu, Z.Y., Chen, H.S., Zhang, W., Xu, Q.X., Wang, S., Wang, K.L., 2015b. Subsurface flow in a soil-mantled subtropical dolomite karst slope: a field rainfall simulation study. Geomorphology 250, 1–14. https://doi.org/10.1016/j.geomorph.2015.08.012.

Goldscheider, N., Chen, Z., Auler, A.S., Bakalowicz, M., Broda, S., Drew, D., Hartmann, J., Jiang, G., Moosdorf, N., Stevanovic, Z., Veni, G., 2020. Global distribution of carbonate

rocks and karst water resources. Hydrogeol. J. 28, 1661–1677. https://doi.org/10.1007/s10040-020-02139-5.
Gowing, J.W., Konukcu, F., Rose, D.A., 2006. Evaporative flux from a shallow watertable: the influence of a vapour–liquid phase transition. J. Hydrol. 321, 77–89. https://doi.org/10.1016/j.jhydrol.2005.07.035.
Guo, X., Jiang, G., Gong, X., Yin, J., Wu, X., 2015. Recharge processes on typical karst slopes implied by isotopic and hydrochemical indexes in Xiaoyan Cave, Guilin, China. J. Hydrol. 530, 612–622. https://doi.org/10.1016/j.jhydrol.2015.09.065.
Guo, Y., Wu, Q., Jiang, G., Han, Z., Tang, Q., Quan, X., 2018. Dynamic variation characteristics of water chemistries and isotopes in a typical karst aquiferous system and their implications for the local karst water cycle, Southwest China. Carbonates Evaporites 34, 987–1001. https://doi.org/10.1007/s13146-018-0457-7.
Hao, S., Li, F., Li, Y., Gu, C., Zhang, Q., Qiao, Y., Jiao, L., Zhu, N., 2019. Stable isotope evidence for identifying the recharge mechanisms of precipitation, surface water, and groundwater in the Ebinur Lake basin. Sci. Total Environ. 657, 1041–1050. https://doi.org/10.1016/j.scitotenv.2018.12.102.
Hartmann, A., Gleeson, T., Wada, Y., Wagener, T., 2017. Enhanced groundwater recharge rates and altered recharge sensitivity to climate variability through subsurface heterogeneity. Proc. Natl. Acad. Sci. 114, 2842–2847. https://doi.org/10.1073/pnas.1614941114.
Hartmann, A., Jasechko, S., Gleeson, T., Wada, Y., Andreo, B., Barbera, J.A., Brielmann, H., Bouchaou, L., Charlier, J.B., Darling, W.G., Filippini, M., Garvelmann, J., Goldscheider, N., Kralik, M., Kunstmann, H., Ladouche, B., Lange, J., Lucianetti, G., Martin, J.F., Mudarra, M., Sanchez, D., Stumpp, C., Zagana, E., Wagener, T., 2021. Risk of groundwater contamination widely underestimated because of fast flow into aquifers. Proc. Natl. Acad. Sci. 118, e2024492118. https://doi.org/10.1073/pnas.2024492118.
Hu, K., Chen, H., Nie, Y., Wang, K., 2015. Seasonal recharge and mean residence times of soil and epikarst water in a small karst catchment of southwest China. Sci. Rep. 5, 10215. https://doi.org/10.1038/srep10215.
Hu, Y., Liu, Z., Zhao, M., Zeng, Q., Zeng, C., Chen, B., Chen, C., He, H., Cai, X., Ou, Y., Chen, J., 2018. Using deuterium excess, precipitation and runoff data to determine evaporation and transpiration: a case study from the Shawan Test Site, Puding, Guizhou, China. Geochim. Cosmochim. Acta 242, 21–33. https://doi.org/10.1016/j.gca.2018.08.049.
Huang, X., Wang, G., Liang, X., Cui, L., Ma, L., Xu, Q., 2017. Hydrochemical and stable isotope (δD and δ18O) characteristics of groundwater and hydrogeochemical processes in the Ningtiaota Coalfield, Northwest China. Mine Water Environ. 37, 119–136. https://doi.org/10.1007/s10230-017-0477-x.
Jiang, G., Guo, F., Lo, K.F.A., Liu, F., Guo, Y., Wu, W., Polk, J.S., 2019. Utilization status of rainwater harvesting and its improvement techniques in bare karst areas for domestic use and ecological restoration. Carbonates Evaporites 34, 1381–1390. https://doi.org/10.1007/s13146-018-0459-5.
Jiang, G., Guo, F., Polk, J.S., Kang, Z., Wu, J., 2015. Delineating vulnerability of karst aquifers using hydrochemical tracers in Southwestern China. Environ. Earth Sci. 74, 1015–1027. https://doi.org/10.1007/s12665-014-3862-9.
Jiang, G., Guo, F., Wu, J., Li, H., Sun, H., 2008. The threshold value of epikarst runoff in forest karst mountain area. Environ. Geol. 55, 87–93. https://doi.org/10.1007/s00254-007-0967-4.
Jiang, G., Liu, F., Wang, Q., Guo, F., 2021. Low impact development construction of peak-cluster depression based on regulation of epikarst zone. Carsologica Sinica. http://kns.cnki.net/kcms/detail/45.1157.P.20210910.1128.002.html.
Kang, Z., Xiong, Z., Li, Y., Ran, J., 2011. The precipitation effect on the water cycle mode of karst subterranean stream catchment. Earth Environ. 39, 26–31.
Kim, K., Lee, X., 2011. Isotopic enrichment of liquid water during evaporation from water surfaces. J. Hydrol. 399, 364–375. https://doi.org/10.1016/j.jhydrol.2011.01.008.
Lee, E., Krothe, N., 2001. A four-component mixing model for water in a karst terrain in south-central Indiana, USA. Using solute concentration and stable isotopes as tracers. Chem. Geol. 179, 129–143.
Li, S., Liu, Y., Her, Y., Chen, J., Guo, T., Shao, G., 2021. Improvement of simulating sub-daily hydrological impacts of rainwater harvesting for landscape irrigation with rain barrels/cisterns in the SWAT model. Sci. Total Environ. 798, 149336. https://doi.org/10.1016/j.scitotenv.2021.149336.
Liu, F., Jiang, G., Wang, J., Guo, F., 2021. The recharge process and influencing meteorological parameters indicated by cave pool hydrology in the bare karst mountainous area. Sustainability 13, 1766. https://doi.org/10.3390/su13041766.
Liu, W., Wang, S., Luo, W., Dai, W., Bai, E., 2017. Characteristics of soil water movement in a grass slope in a karst peak-cluster region, China. Hydrol. Process. 31, 1331–1348. https://doi.org/10.1002/hyp.11105.
Ma, B., Liang, X., Liu, S., Jin, M., Nimmo, J.R., Li, J., 2017. Evaluation of diffuse and preferential flow pathways of infiltrated precipitation and irrigation using oxygen and hydrogen isotopes. Hydrogeol. J. 25, 675–688. https://doi.org/10.1007/s10040-016-1525-5.
Mao, H., Wang, G., Shi, Z., Liao, F., Xue, Y., 2021. Spatiotemporal variation of groundwater recharge in the lower reaches of the Poyang Lake Basin, China: insights from stable hydrogen and oxygen isotopes. J. Geophys. Res. Atmos. 126, e2020JD033760. https://doi.org/10.1029/2020jd033760.
Masiol, M., Zannoni, D., Stenni, B., Dreossi, G., Zini, L., Calligaris, C., Karlicek, D., Michelini, M., Flora, O., Cucchi, F., Treu, F., 2021. Spatial distribution and interannual trends of δ18O, δ2H, and deuterium excess in precipitation across North-Eastern Italy. J. Hydrol. 598, 125749. https://doi.org/10.1016/j.jhydrol.2020.125749.
Peng, T., Wang, S.-J., 2012. Effects of land use, land cover and rainfall regimes on the surface runoff and soil loss on karst slopes in southwest China. Catena 90, 53–62. https://doi.org/10.1016/j.catena.2011.11.001.
Perrin, J., Jeannin, P.-Y., Zwahlen, F., 2003. Epikarst storage in a karst aquifer: a conceptual model based on isotopic data, Milandre test site, Switzerland. J. Hydrol. 279, 106–124. https://doi.org/10.1016/s0022-1694(03)00171-9.
Pfahl, S., Sodemann, H., 2014. What controls deuterium excess in global precipitation? Clim. Past 10, 771–781. https://doi.org/10.5194/cp-10-771-2014.
Qin, L., Bai, X., Wang, S., Zhou, D., Li, Y., Peng, T., Tian, Y., Luo, G., 2015. Major problems and solutions on surface water resource utilisation in karst mountainous areas. Agric. Water Manag. 159, 55–65. https://doi.org/10.1016/j.agwat.2015.05.024.
Qiu, J., Jiang, Y., Lv, T., Mao, Y., Wu, Z., Ma, L., Wang, Q., Zhang, C., 2022. Response of stable isotopes of hydrogen and oxygen in soil water and groundwater to tunnel construction in typical karst trough valley. Earth Sci. 47 (02), 717–728.
Solder, J.E., Beisner, K.R., 2020. Critical evaluation of stable isotope mixing end-members for estimating groundwater recharge sources: case study from the South Rim of the Grand Canyon, Arizona, USA. Hydrogeol. J. 28, 1575–1591. https://doi.org/10.1007/s10040-020-02194-y.
Sprenger, M., Leistert, H., Gimbel, K., Weiler, M., 2016. Illuminating hydrological processes at the soil-vegetation-atmosphere interface with water stable isotopes. Rev. Geophys. 54, 674–704. https://doi.org/10.1002/2015rg000515.
Uber, M., Vandervaere, J.-P., Zin, I., Braud, I., Heistermann, M., Legoût, C., Molinié, G., Nord, G., 2018. How does initial soil moisture influence the hydrological response? A case study from southern France. Hydrol. Earth Syst. Sci. 12, 6127–6146. https://doi.org/10.5194/hess-2018-28.
Wang, F., Chen, H., Lian, J., Fu, Z., Nie, Y., 2020a. Hydrological response of karst stream to precipitation variation recognized through the quantitative separation of runoff components. Sci. Total Environ. 748, 142483. https://doi.org/10.1016/j.scitotenv.2020.142483.
Wang, F., Chen, H., Lian, J., Fu, Z., Nie, Y., 2020b. Seasonal recharge of spring and stream waters in a karst catchment revealed by isotopic and hydrochemical analyses. J. Hydrol. 591, 125595. https://doi.org/10.1016/j.jhydrol.2020.125595.
Wang, S., Fu, Z., Chen, H., Nie, Y., Xu, Q., 2020c. Mechanisms of surface and subsurface runoff generation in subtropical soil-epikarst systems: implications of rainfall simulation experiments on karst slope. J. Hydrol. 580, 124370. https://doi.org/10.1016/j.jhydrol.2019.124370.
Williams, P., 2008. The role of the epikarst in karst and cave hydrogeology: a review. Int. J. Speleol. 37, 1–10.
Xu, Y., Wang, J., Gao, X., Zhang, Y., 2018. Application of hydrogen and oxygen stable isotope techniques on soil water research: a review. J. Soil Water Conserv. 32, 1–9.
Yan, Y., Dai, Q., Yuan, Y., Peng, X., Zhao, L., Yang, J., 2018. Effects of rainfall intensity on runoff and sediment yields on bare slopes in a karst area, SW China. Geoderma 330, 30–40. https://doi.org/10.1016/j.geoderma.2018.05.026.
Yuan, D., 2014. Regional Problems on Environmental Geology in South and Southwest China and Their Count Measurement. Science Press, Beijing, China.
Zhang, T., Li, J., Pu, J., Huo, W., Wang, S., 2021. Spatiotemporal variations of soil water stable isotopes in a small karst sinkhole basin. Environ. Earth Sci. 80, 29. https://doi.org/10.1007/s12665-020-09284-w.
Zhao, M., Hu, Y., Zeng, C., Liu, Z., Yang, R., Chen, B., 2018. Effects of land cover on variations in stable hydrogen and oxygen isotopes in karst groundwater: a comparative study of three karst catchments in Guizhou Province, Southwest China. J. Hydrol. 565, 374–385. https://doi.org/10.1016/j.jhydrol.2018.08.037.
Zhou, X., Jin, X., Liang, S., Shen, Y., Zhang, H., 2017. Specialized Groundwater Sciences. 2nd edition. Geological Publishing House, Beijing, China.